Effect of engine conditions and injection timing on piston-top fuel films for stratified direct-injection spark-ignition operation using E30

Carl-Philipp Ding[1], David Vuilleumier[2], Namho Kim[2], David L Reuss[2], Magnus Sjöberg[2] and Benjamin Böhm[1]

Abstract

Mid-level ethanol/gasoline blends can provide knock resistance benefits for stoichiometric spark-ignition engine operation, but previous studies have identified challenges associated with spray impingement and wall wetting, leading to excessive particulate matter emissions. At the same time, stratified-charge spark-ignition operation can provide increased thermal efficiency, but care has to be exercised to avoid excessive in-cylinder soot formation. In support of the use of mid-level ethanol/gasoline blends in advanced spark-ignition engines, this study presents spray and fuel-film measurements in a direct-injection spark-ignition engine operated with a 30 vol.%/70 vol.% ethanol/gasoline blend (E30). Crank-angle resolved fuel-film measurements at the piston surface are conducted using two different implementations of the refractive index matching technique. A small-angle refractive index matching implementation allows quantification of the wetted area, while a large-angle refractive index matching implementation enables semi-quantitative measurements of fuel-film thickness and volume, in addition to fuel-film area. The fuel-film measurements show that both the amount of fuel deposited on the piston and the shape of the fuel-film patterns are strongly influenced by the injection timing, duration, intake pressure, and coolant temperature. For combinations of high in-cylinder gas density and long injection duration, merging of the individual spray plumes, commonly referred to as spray collapse, can cause a dramatic change to the shape and thickness of the wall fuel films. Overall, the study provides guidance to engine designers aiming at minimizing wall wetting through tailored combinations of injection timings and durations.

Introduction

Future internal combustion engines have to meet stringent emission and efficiency targets, providing motivation for research efforts of advanced combustion engine concepts that have potential for higher efficiency than conventional engines. Since the engine is only one link in the chain of providing useful work, from a CO_2 perspective there is also motivation to examine the use of advanced fuels that are based on renewable resources and/or contribute to optimized refinery operations. Advanced fuels can also provide improved combustion characteristics, which can facilitate meeting efficiency and emission targets. This leads to the current investigation of an advanced combustion concept (i.e. stratified direct-injection spark-ignition (DISI) operation) with

new fuels—in this case an E30 blend of ethanol with gasoline (30 vol.%/70 vol.%).[1,2]

DI strategies offer a potential to improve thermal efficiencies. For part-load operation, stratified-charge offers reduced pumping losses by de-throttling and improvements to the specific heat ratio of the working fluid. The engine load is controlled by the charge fuel-

[1]Fachgebiet Reaktive Strömungen und Messtechnik (RSM), Technische Universität Darmstadt, Darmstadt, Germany
[2]Sandia National Laboratories, Livermore, CA, USA

Corresponding author:
Magnus Sjöberg, Sandia National Laboratories, P.O. Box 969, MS 9053, Livermore, CA 94551-0969, USA.
Email: mgsjobe@sandia.gov

loading provided by high-pressure fuel injection. Proper mixture preparation prior to and during flame propagation is important to provide reliable ignition and reduce emissions.

Engine-out particulate matter (PM) is the net result of soot formation and oxidation in the bulk gas and can occur without wall wetting. For example, a study by Zeng et al.[3] demonstrates that non-ideal gas flows can cause increased bulk-gas soot formation and elevated smoke for stratified-charge SI operation. Fuel impingement on combustion chamber surfaces and the resultant wall wetting can be a problem for stratified SI operation since the fuel is injected during the later stages of compression when the piston is approaching top dead center (TDC), sometimes with a short distance between the injector and the piston top, as compared to standard intake stroke injection strategies.[2] Even though the resultant fuel films are thin, typically in the order of single micrometer, and comprise a small volume of the total injected fuel, the short time span between injection and combustion means that these films may be present during the combustion event.[4,5] Direct numerical simulations have shown that the thickness of such fuel films decreases by a few tenths of a micrometer during a flame–wall interaction scenario which took place within a few milliseconds.[6] Such fuel films lead to fuel-rich regions at the piston surface which burn as diffusive flames. These non-premixed flames are known as pool fires and have often been visualized by direct flame imaging of their bright yellow emission.[4,7] Stevens and Steeper[7] imaged soot production from such pool fires using laser elastic scattering and observed that soot produced by the pool fires persisted throughout the expansion stroke when the burnt gas temperature is already decreasing and being too low to further oxidize the formed soot. This results in increased levels of tail pipe soot emissions. For this reason, spray impingement on the piston or any other surface of the cylinder needs to be prevented within SI engines.

Fuel injectors used in DISI engines are designed to provide the desired penetration, droplet size distribution, and fuel–air mixing while avoiding wall wetting. However, engine parameters such as the in-cylinder gas pressure and temperature during injection, as well as the in-cylinder flow, have a strong influence on the spray characteristics.[8] Multi-hole gasoline direct-injectors are prone to spray–plume interactions. The extreme manifestation of plume interaction is "spray collapse," where all plumes merge to a single plume. Light scattering (the label "light scattering" is used to include all elastically scattered light as well as light reflection and/or refraction by large-scale droplets and window-surface roughness) and Schlieren imaging used to capture the macroscopic features of the spray revealed that spray collapse can occur at increased ambient pressures,[9] conditions which are found during late injection. The separation of the plumes was observed to progressively decrease during the injection event in cases of spray collapse. A detailed investigation of mixing based on laser-induced fluorescence (LIF) and Rayleigh scattering showed that the plumes start to merge earlier after the start of injection (SOI) for increasing ambient densities.[10] This transient behavior of the individual plumes during spray collapse was confirmed by Sphicas et al.[11] They performed time-resolved measurements of the surrounding flow field using particle image velocimetry (PIV) and showed that ambient gas is entrained axially from the bottom of the spray as well as radially through the gap in between the plumes at SOI. Once the neighboring plumes start to interact, this gap closes and the angle between the plumes continuously decreases until the final spray collapse. Another cause for detrimental changes of the spray pattern are injector deposits which can reduce the injector fuel flow rate and cause changes to the desired spray patterns, such as changed spray angle, prolonged spray penetration distance, asymmetric spray envelope, and larger spray droplet diameter.[12] A direct comparison of a clean and coked injector by high-speed imaging for the characterization of macroscopic spray characteristics and LIF of spray footprint carried out by Badawy et al.[13] showed that the injector deposits reduced plume cone angle while plume penetration length and plume separation angles increased.

Although the physical phenomena underlying spray collapse and non-ideal/aberrant spray behavior are beginning to be understood, the interactions between spray phenomena and fuel impingement in a complex (non-idealized) engine environment are not sufficiently documented in the literature. Specifically, measurements of fuel films on surfaces are desirable, as films distinctly represent one form of imperfections of the mixture formation. Fuel-film information provides an understanding of the practical importance of problems such as spray collapse, and the resulting emissions and efficiency implications of these problems. Such information also supports the development of spray impingement models, which may have an important role in correctly predicting the emissions from gasoline direct injection (GDI) engines.

For time-resolved two-dimensional quantitative fuel-film measurements, LIF and refractive index matching (RIM) are suitable (see Henkel et al.[14] for a recent overview). LIF has been applied at ambient conditions,[15] vessels,[16,17] and rapid compression machines.[18] For such measurements, the spectral characteristics of the fuel has to be well known and the film thickness needs to be relatively thick in the order of tens of micrometers.[19] The applicability of this technique is further limited due to background signal of the fuel vapor and the pressure dependency of the LIF signal.[20] RIM was first demonstrated by Drake et al.[4] in a DISI engine. This technique was used to investigate fuel films on the piston surface as a possible source of smoke and hydrocarbon emissions. Since the introduction of this technique, the calibration procedure needed for quantitative RIM measurements has been refined, and possible error

sources have been discussed in more detail, for example, the influence of the fuel's refractive index on the RIM signal.[5,21,22] For this study, spray imaging and RIM are used in a motored DISI engine to reveal operating conditions that produce fuel impingement and fuel-film formation on the piston. Focus is on stratified-charge operating strategies that use fuel injection during the late compression stroke. Spray imaging shows the dynamic spray evolution leading to piston impingement in this engine (having asymmetric geometry, gas-phase momentum, and time-dependent density), which changes with operating conditions. RIM is used first as an unambiguous detector of liquid fuel impingement onto the bottom surface of the piston bowl. Also, the RIM images are analyzed to estimate the fuel-film area and volume, metrics which reveal systematic changes with engine operation. Specifically, changes in the fuel films are documented as the intake pressure (P_{in}), injection timing, and injection duration are changed systematically. The experimental results also include the effects of a reduced coolant temperature, which represents engine conditions during an engine warm-up phase.

Experimental setup

Engine and operating conditions

This investigation was conducted in an optical DISI engine at Sandia National Laboratories, shown in Figure 1 and fully documented by Zeng et al.[8] The engine has an extended Bowditch type piston and can operate in two configurations, an all-metal configuration for continuously fired performance testing or in an optical configuration with quartz windows in the piston bowl and pent-roof gables. This study only uses the optical configuration. The four-valve pent-roof combustion chamber had one intake valve deactivated to increase swirl, which was shown to provide repeatable combustion for stratified operation in the previous testing.[23]
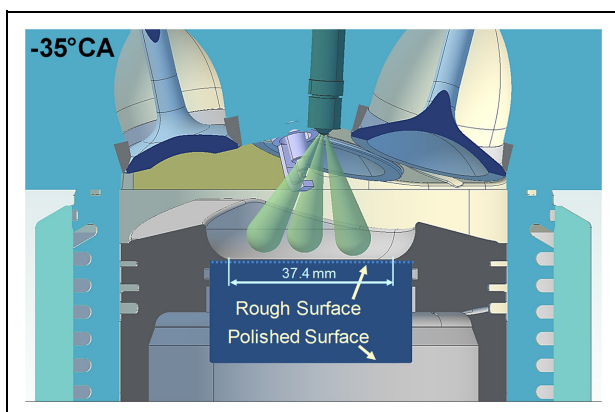

Figure 1. Cross-sectional view of the combustion chamber at −35 °CA. The rough surface of the quartz window provides a 37.4 mm view for wall-film measurements.

The piston bowl and eight-hole injector are slightly offset from the cylinder axis, and the injector is inclined 5° from vertical. The injector produces eight spray plumes in a circular pattern, nominally being symmetric with respect to the injector axis. The injector has a 60° included angle based, as documented by Blessinger et al.[10] A gasoline with 30% ethanol (E30), was chosen for these tests partly because this particular fuel has been shown to generate higher smoke level than other gasoline fuels under engine operating conditions where pool fires are the main source of soot emission. This fuel also has a tendency to produce high smoke levels under conditions of low coolant temperature.[24] This E30 fuel is one of the Co-Optima Core fuels, sharing a common research octane number (RON) of 98, and being well documented by Fouts et al.[25] Selected fuel properties are listed in Table 1. This E30 fuel is also of interest given the trend that fuels with an increasing amount of ethanol blended with gasoline are becoming available in the market. A summary of the engine geometry and operating conditions are provided in Table 2. It should be noted that all given crank angle degrees (°CA) are referenced to TDC combustion, using negative numbers for the compression stroke.

Figure 2 shows how the amount of injected fuel varies with the duration of the electrical command provided to the injector driver. For the purpose of comparing the spray images in this study with static-vessel spray behavior, the in-cylinder gas density, pressure, and temperature are plotted in Figure 3. The spray and RIM measurements were acquired while the engine was motored without combustion, using a repeating skip-injection scheme: five cycles without injection and one cycle with injection.

Spray imaging

The high-speed imaging of the fuel films in these RIM tests revealed that the fuel films were localized regions, whose appearance on the piston was separated spatially and temporally. Attempts to interpret the RIM results lead to the speculation that the sprays can experience the "collapsing" phenomenon observed by Sphicas et al.[11] This interpretation of the RIM results motivated the use of spray imaging to document the nature of the spray evolution at the different operating conditions. The spray imaging was conducted in a separate set of experiments at the same engine operating conditions as the RIM measurements.

Light scattered from the liquid spray was imaged through the pent-roof window and a normal polished piston window. The camera for imaging the spray via the pent-roof window (cf. v710 in Figure 4(a)) was tilted downward to have better access to the spray inside the piston bowl (cf. Figure 4(b)). Two high-speed light-emitting diodes (LEDs) were used for spray illumination. Both cameras were operated at 20 kHz, which corresponds to 0.3 °CA. The resolution of Phantom v710 and v611 cameras were 496 × 360 and

Table 1. Selected fuel properties of the E30 fuel used in this study.

|	
RON	97.9
MON	87.1
Octane sensitivity	10.8
AKI	92.5
Oxygenates (vol.%)	30.6
Aromatics (vol.%)	13.8
Alkanes (vol.%)	40.5
Cycloalkanes (vol.%)	7.0
Olefins (vol.%)	5.6
T10 (°C)	61
T50 (°C)	74
T90 (°C)	155
Net heat of combustion (MJ/kg)	38.2
HoV (kJ/kg)	532.4
AFR stoichiometric	12.9
HoV (kJ/kg stoichiometric charge)	38.4
Liquid density at 15 °C (g/mL)	0.7527
Index of refraction (-)	1.400

RON: research octane number; MON: motor octane number; AKI: anti-knock index; AFR: air-to-fuel ratio; HoV: heat of vaporization.

Table 2. Summary of engine geometry and operating conditions.

Bore/stroke, mm	86/95.1
Displacement, L	0.552
Compression ratio	12:1
Engine speed, r/min	1000
Coolant temperature, °C (unless noted otherwise)	90
Intake temperature, °C	30
Intake pressure, kPa	100 and 130
Injection pressure, MPa	17
Injection timing, actual (SOI$_a$) aTDC, °CA	−41 to −6
Density at SOI$_a$, 100 kPa, kg/m^3	4.6 to 11.9
Density at SOI$_a$, 130 kPa, kg/m^3	5.9 to 15.3
Injection duration, μs	400 to 1600
Injected mass, mg/cycle	4.2 to 21.3

SOI: start of injection; aTDC: after top dead center.
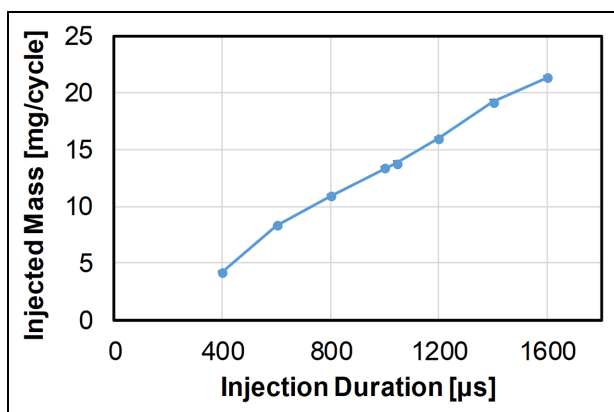
Figure 2. Injected mass per cycle plotted against electrical injection duration.

368 × 360, respectively. Two LEDs were used for illuminating the spray and each LED was dedicated to each camera for imaging sprays from different views.
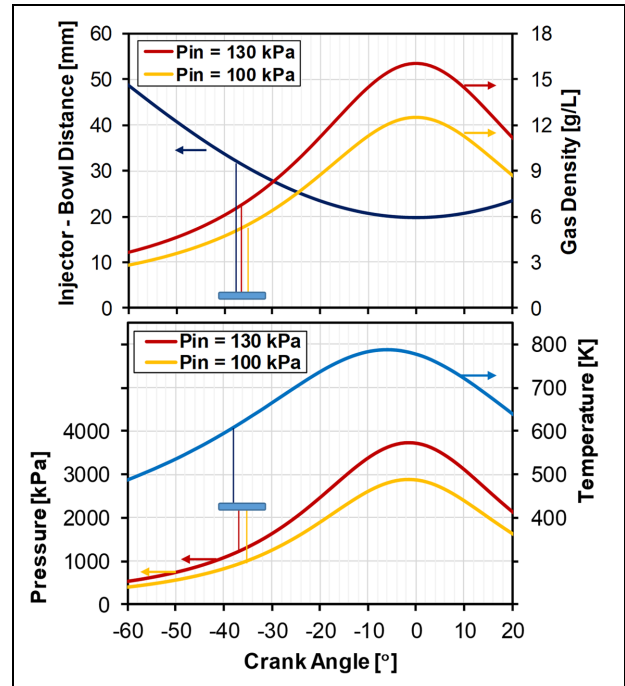
Figure 3. Injector-to-bowl distance and estimated in-cylinder gas density, temperature, and pressure during the late compression stroke and around TDC. Coolant temperature = 90° C. As an example, the blue annotations indicate the injection duration for operation with SOI$_a$ = −41 °CA and an electrical command of 1600 μs.

Both LEDs were operated in a pulsed mode with 2 μs pulse duration. One LED located near the pent-roof provided illumination for the camera at the bottom (cf. v611 in Figure 4(a)), delivering 7 μJ/pulse. The other LED installed near the Bowditch mirror provided illumination for the camera near the pent-roof window (cf. v710 in Figure 4(a)), delivering 20 μJ/pulse. To avoid reflections of LED illumination, the LED light pulses and associated camera exposure windows were separated by 6 μs. This led to a deviation in the recording time of the spray by 6 μs. However, 6 μs is about an order of magnitude shorter time compared to the time in between each frame, which is 50 μs for the 20 kHz frame rate used in this study. Thus, to simplify the interpretation, the time and CA stamps in the presented spray images are kept the same for the two cameras.

RIM measurements

Refractive-index-matching imaging was developed for high-speed two-dimensional measurements of fuel films, as well as the quantification of fuel-film area and volume.[4,5,21,22] The principle of RIM is explained with the two optical configurations used in this study, as illustrated in Figure 5. In either configuration, the top surface of the piston window was roughened and illuminated by a light source. The illumination and imaging for both configurations are from the exterior of the window (through the extended piston), thus imaging the back-scattered and back-reflected light from
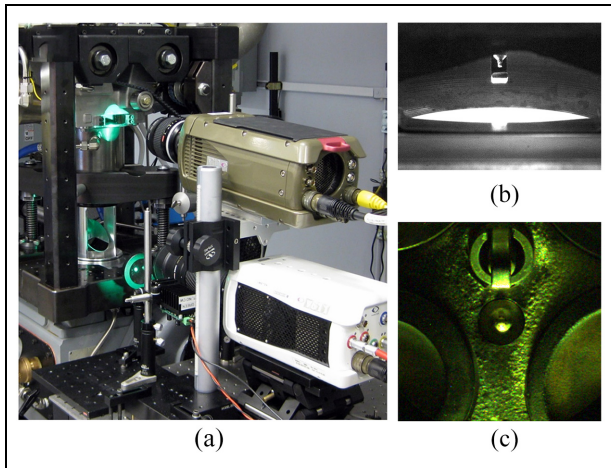
Figure 4. Optical setup (a) and fields of view for simultaneously imaging liquid spray scattering through both the pent-roof (b) and piston (c). Piston view is the same for both the spray and RIM images. Note that while (a) shows a horizontal orientation of the upper Phantom camera, for the data acquired in this study that camera was tilted down slightly to provide a view (b) into the bowl.
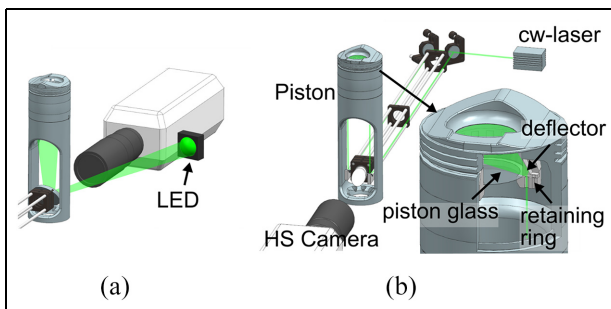

Figure 5. Optical setup of piston fuel-film measurements: (a) small-angle refractive index matching (SA-RIM) and (b) large-angle refractive index matching (LA-RIM).

the roughened surface. However, the detected RIM signal depends on the incident angle of the light, as described below. In either case, fuel impingement fills

the surface irregularities partly or fully, thereby changing the amount of transmitted, reflected, and scattered light, as illustrated in Figure 6(a).

Small-angle refractive index matching. In this small-angle RIM implementation, the LED light source is located near the camera lens, as shown in Figure 5(a). The surface roughness is also quite small with $R_a = 0.32 \, \mu m$, contributing to a high detection sensitivity. The desired roughness was achieved by not proceeding to the final polishing step in the manufacturing process of the quartz window. When fuel impinges on the lightly roughened surface, it quickly fills the surface irregularities, either partly or fully. Since the liquid fuel has a refractive index close to the glass (compared to the surrounding gas), the light paths at the surface change. The fuel film effectively creates a smoother interface between the glass and the gas, thereby reducing the amount of light that is scattered randomly. Consequently, both the transmitted and back-reflected light increase. Because the amount of back-reflected light detected by the camera is sensitive to both the illumination and viewing angles, as well as the local orientation of the fuel film, the amount of light that reaches the camera does not vary monotonically with fuel-film thickness, as can be gleaned from Figure 6(b). In addition, the detected amount of light varies with the location of the fuel film on the window. For these reasons, small-angle refractive index matching (SA-RIM) cannot be used to quantify the thickness of the fuel film. However, the setup is simple and it can be used as a sensitive detector that reveals the location and shape of the fuel film. With appropriate post-processing, SA-RIM can also be used to quantify the size of the wetted area, but this is outside the scope of this study. A Phantom v611 color camera was used for all measurements—this is the same camera used for the bottom-view spray imaging. For the SA-RIM measurements presented in conjunction with spray imaging, the frame rate was 10 kHz (corresponding to 0.6 °CA), using an exposure of 95 μs, with a green LED in continuous mode. For all other SA-RIM results, the frame
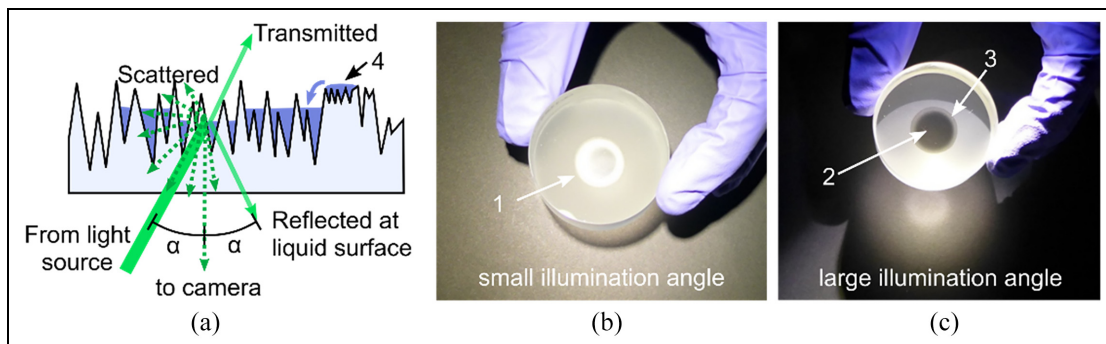

Figure 6. Illumination of liquid films at a rough glass surface. (a) Illustration of light scattering, reflection, and transmission at the rough surface with a small liquid film. Calibration samples using a (b) small illumination angle, SA-RIM, and (c) large illumination angle, LA-RIM.

rate was 3 kHz (corresponding to 2 °CA), using an exposure of 300 μs, and with the LED in continuous mode.

Large-angle refractive index matching. The current large-angle RIM implementation is identical to the one used in Ding et al.[5] and illustrated in Figure 5(b). Because of the large incident angle of the light on the roughened surface, a specular reflection back to the camera is generally avoided. Without fuel on the roughened surface, the camera detects mostly diffusively scattered light. When fuel deposits on the surface, transmission into the combustion chamber increases, leading to a reduction of the backscattered light as illustrated in Figure 6(c). In the engine, this RIM phenomenon unambiguously defines the time and location of fuel impingement. Estimation of the fuel-film boundaries, and thus area, is performed with image processing edge detection. Estimation of the deposited fuel volume and evaporation rates are achieved by empirical calibration of the film "thickness," h, (actually the volume per unit area) as a function of light intensity within the film area

$$h(x, y) = \frac{I_{inj}(x, y)}{I_{ref}(x, y)} \quad (1)$$

where I_{ref} is the intensity at the image pixel in the absence of the fuel film and I_{inj} is the intensity of the image after fuel impingement. For these tests, I_{ref} comes from a reference image that is the average of reference images that were acquired on the cycles before the injected cycles, matching the crank angle to the image with injection being analyzed. It is intuitive that h(I) is a considerably complex function of the illumination source characteristics, collection optics, surface roughness characteristics, film wetting characteristics, refractive indices (n_{gas}, n_{film}, and n_{window}), and any secondary scattering of light from within the engine cylinder. This drives the need for empirical calibration of the function.

The average roughness of the top glass surface was $R_a = 6.3$ μm (details are given in Ding et al.[5]). This is a much rougher surface compared to the SA-RIM implementation and is driven by the desire to provide thickness quantification in micrometer range. This high roughness was achieved by sandblasting a normal polished window. As long as the film thickness is a fraction of R_a, the ratio of backscattered light intensity before and after the liquid film deposition can be utilized to determine the local amount of liquid on the surface. A film thicker than the surface roughness causes the backscatter to become small and insensitive to the liquid film thickness. This saturation effect limits the range of the film thickness measurement to a fraction of R_a.

All large-angle refractive index matching (LA-RIM) experiments employed laser illumination by directing a 532 nm, 90 mW, CW laser beam through the extended piston port, deflected from two sides of the piston (providing a large angle of incidence) and expanded as illustrated in Figure 5(b); thus, labeled here as large-angle illumination, LA-RIM. The vertical paths of the laser beams are aligned to the axis of the piston, so that the illumination of the piston surface is independent of the piston position. The laser intensity was sufficient to allow an exposure time of 300 μs, using a camera frame rate of 3 kHz (2 °CA division). SA-RIM and LA-RIM intensity distributions are different as demonstrated with the calibration samples of Figure 6(b) and (c). In this study, the LA-RIM is used for the fuel-film area and volume quantification measurements. More details of the LA-RIM system are provided by Ding et al.[5]

The calibration to compute the film height function, h(I), in equation (1) is a combination of the techniques described in the studies by Drake et al.[4] and Maligne and Bruneaux.[22] The calibration tests were performed at room temperature and pressure with the same piston window used in the engine tests. In brief, the calibration was performed by applying a known volume of isooctane and dodecane mixtures to the piston window with a syringe. Movies were recorded of the light intensity within the fuel-film region as the fuel evaporated (cf. Figure 7). The recorded backscattered light intensity first decreases rapidly, due to index matching, as the applied fuel spreads to a thin film. Then the intensity increases rapidly toward the original intensity, I_{ref}, value as the isooctane evaporates. After all the isooctane has evaporated, the intensity increases more slowly due to the slower evaporation rate of dodecane. The intensity at the inflection point between isooctane and dodecane evaporation is the intensity value corresponding to the height of the dodecane film (volume per unit area). To produce the intensity function at different volumes, tests were repeated with the same total volume of the mixture while systematically varying proportion of isooctane to dodecane. A detailed account of this calibration procedure is provided by Ding et al.[5] The resulting function is given in equation (2) and plotted in Figure 8.
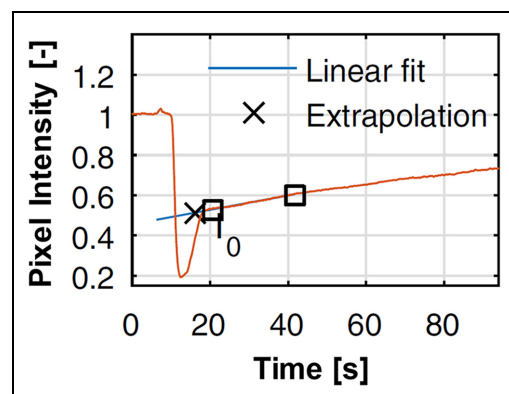

Figure 7. Example of light intensity change during evaporation of fuel applied for the calibration.
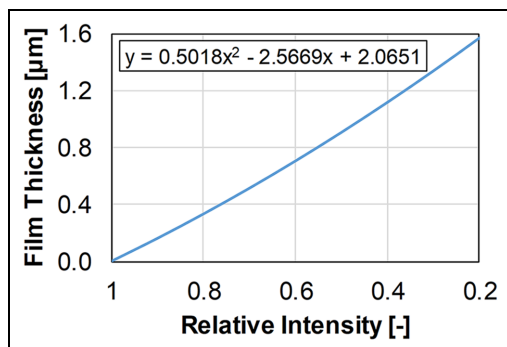
Figure 8. Calibration polynomial of the LA-RIM measurements.

$$h(x, y) = 0.50179 \times \left(\frac{I_{inj}(x, y)}{I_{ref}(x, y)} \right)^2$$
$$-2.5669 \times \frac{I_{inj}(x, y)}{I_{ref}(x, y)} + 2.0651 \tag{2}$$

Uncertainty of RIM area and volume measurements

In-cylinder RIM images were acquired with skip-injection operation, using a repeating sequence of five non-injected cycles followed by one injected cycle. Both the measurement and reference images were spatially averaged with a 12×12 pixel ($0.7\,mm \times 0.7\,mm$) filter, then analyzed pixel by pixel. The reference image, $I_{ref}(x, y)$, was further averaged over 20 images acquired in the cycles just prior to the injected cycles. Analysis of the first and last reference images from the tests shows no significant changes. To locate the regions where fuel deposition occurred, measurement images were binarized using the value of $h(x, y) = 0.1\,\mu m$ as the threshold value, which is the noise level based on histograms of the cycles without injection. Thus, the uncertainty of the fuel-film area computed from the RIM images is dependent on the size of the area and the uncertainty of the boundary location, which is on the order of $0.5\,mm$ due to the application of the 12×12 pixel filter.

Uncertainty of the RIM volume is determined by the uncertainty in the empirical calibration of h, plus additional factors occurring in the engine. The uncertainty of the applied liquid-mixture volume, $0.6\,\mu L$, is less than 1.5% based on the $\pm 0.01\,\mu L$ resolution of the syringe, a statistical uncertainty (imprecision) that is reduced by multiple tests and small compared to the other sources of inaccuracy. Another source of inaccuracy is the spatial variation of the surface roughness, which was shown to have a standard deviation of 8%.[5] During the calibration, the effect of this is minimized using averaging. Nonetheless, the spatial variation of the roughness contributes directly to the in-cylinder measurements since the fuel-film locations vary from test to test. The 8% spatial variation of surface roughness is assumed to contribute linearly to the uncertainty of the calculated liquid volume for these estimates.

The absolute accuracy of the calibrated height function, h, is affected by dodecane evaporation prior to the calibration image, which was recorded at the end of the isooctane evaporation period (inflection point in Figure 7). To address this,[5] the dodecane is assumed to evaporate during the initial isooctane evaporation period at the same rate as the post isooctane period, the rate computed by a linear fit between the two square markers in Figure 7. The intensity for each calibration test image is taken to be the value extrapolated to the time halfway between the start of liquid application and the end of isooctane evaporation image (the x marker in Figure 7). The inaccuracy is estimated to be 10%, based on the observed slopes of the area-average intensity before and after the calibration point as shown in Figure 7.

The absolute accuracy of the in-cylinder measurements is affected further by differences in the refractive index, n, between dodecane and the multicomponent E30 fuel. It is likely that the composition, and thus the refractive index, of the fuel-film is not necessarily the same as the injected fuel. This inaccuracy was addressed by testing eight single components of the E30 with a range of refractive indices.[5] An absolute inaccuracy is estimated to be up to 15%.

This analysis demonstrates that the absolute accuracy of fuel-film volume dominates the uncertainty of the area and volume measurements. Assuming that the given error sources are uncorrelated, the total uncertainty of the liquid volume calibration is approximately 20%. This estimation has to be considered the best possible and caution should be exercised for any direct comparison with computational fluid dynamics (CFD) results, for example. Nonetheless, the precision of the volume measurement is adequate and convenient to quantify fuel-film area and volume trends across the operating spectrum studied here.

In summary, the height uncertainty is 20%, dominated by the calibration uncertainty and refractive index uncertainty, which are constant for all height image intensities. Therefore, the volume uncertainty as a percentage of the measurement varies with the area. For a 4-mm diameter circular spot with a $0.5\,mm$ measurement error (typical of a single-plume impingement here), the area uncertainty is 10% for a single measurement and of course less when averaging over multiple spots, multiple images, and larger areas.

Two final cautions are considered. First, Ding et al.[5] have shown that the volumes for film thicknesses above $0.9\,\mu m$ can be significantly underestimated for the window surface roughness used in this LA-RIM implementation. Finally, RIM volumes computed during the presence of the spray will contain secondary light

scattering from airborne liquid droplets (not present when recording the reference image), which will tend to increase the intensity and therefore underpredict the volume.

Results and discussion

The fuel impact and subsequent film formation are affected by the character of the sprays. Thus, an interpretation of the RIM results first requires an understanding of the spray evolution during the injection event. A summary of the spray evolution as revealed in quiescent-chamber studies conducted by other researchers is provided first. The results here focus on the effect of operating conditions on fuel impingement on the piston. For brevity, a single example of spray imaging and SA-RIM evolution from this study is used to illustrate the in-cylinder spray evolution and its impingement on the piston. This is followed by recording the fuel-film patterns, area, and volume changes with changes in late injection timing, injection duration, and P_{in} (100 and 130 kPa). With the exception of section "Effect of coolant temperature," all results presented are for an engine coolant temperature of 90° C.

Spray development and fuel impingement

Studies in quiescent chambers have demonstrated that the sprays from multi-hole injectors (in the absence of flash boiling at high fuel temperature and low ambient-gas pressure) initially create a hollow-cone spray, that is, a conical curtain of individual spray jet plumes. The plumes can remain separate or merge and "collapse" as observed by Parrish et al.,[9] depending on ambient conditions and injection characteristics. Sphicas et al.[11] provide a comprehensive state-of-the-art review and description of the temporal evolution of the Engine Combustion Network (ECN) Spray G multi-hole gasoline injector, which is generically similar to the injector used here. In brief, the initially individual plumes broaden and can merge to the extent that scattered-light imaging shows liquid spray which appears to "collapse." There are two entrainment processes occurring during the evolution to spray collapse. One is the entrainment of the ambient gas into the individual jets that broadens and disperses the droplets of the individual jets. At some ambient density and temperatures, there is sufficient dispersion that the jets can merge. The interior angle of the plumes, initially determined by the direction of the injector holes, is observed to decrease during the injection leading to the observed collapse at some conditions. The second entrainment process is larger spatial-scale entrainment of the droplets to the interior of the spray curtain, caused by the low-pressure and reverse radial and axial flow along the spray-curtain centerline. Thus, the initially hollow-cone spray now has liquid entrained into the interior region. As the individual plumes disperse, the outside cone angle of the remaining "interior" droplets appears

smaller, which is described as the apparent spray "collapse" observed from the outside of the spray curtain.[9,11] Discrimination between the two entrainment processes is made here to aid in the interpretation of the fuel-film formation discussed later.

The same physical processes observed in the chambers are observed for the in-cylinder sprays in this study, although modified by the variable density, in-cylinder flow, and piston bowl. Figure 9 provides one example of the spray development and resulting wall wetting. The combination of $SOI_a = -31$ °CA, $P_{in} = 100$ kPa, and a long injection duration of 1600 μs was selected since it allows a discussion of all the important spray dynamics. The left two columns of Figure 9 show images of light scattering recorded from the side and through a polished window in the bottom of the piston bowl, respectively. The images are unprocessed (except as noted) and extracted from movies recorded simultaneously during a single cycle. The initial spray at this condition (-30.6 °CA) shows individual plumes on trajectories principally defined by injector hole centerlines. This was true of all operating conditions tested here, that is, no flash boiling. These spray plumes remain symmetric and on their original trajectory, each appearing to grow larger (radially) as the droplets are dispersed by entrainment into the jets (cf. -27.9 °CA). By -26.7 °CA, the dispersion of the individual plumes show asymmetry, the first indication that the in-cylinder flow is affecting the entrainment. This, of course, is not observed in the quiescent vessel but was observed in this engine during the in-cylinder study of Zeng et al.[23] By -24.9 °CA, two plumes have merged (7–8 o'clock, bottom view), showing further asymmetry due to in-cylinder flow. After the end of injection, -19.5 °CA, the spray plumes no longer exist and only the liquid convected into the interior of the otherwise hollow cone remains. Slight evidence of this interior liquid lasted until -18.3 °CA with this illumination and image sensitivity. Previous studies have labeled the transition from the liquid plumes to the interior liquid as spray collapse, implying a convection of material.[9,11] However, it cannot be ruled out that once the plumes have disappeared (not being fed by injected liquid jets), the interior liquid is locally saturated and requires entrainment of fresh air for evaporation as well as convective motion of the liquid.

The formation of fuel films during the injection event can be observed in the unprocessed SA-RIM images in the right column of Figure 9. The top two SA-RIM images (-30.6 and -27.9 °CA) show secondary scattered light from the spray above the piston window. The roughened surface obfuscates the image but still adds intensity to the images that is not present when the reference images are recorded. Therefore, this secondary scattered light is not subtracted by the reference images and affects the estimated film height during crank angles when the airborne liquid is present.

The first impact of liquid from the spray plumes can be observed -26.7 °CA, as the small bright spots at the
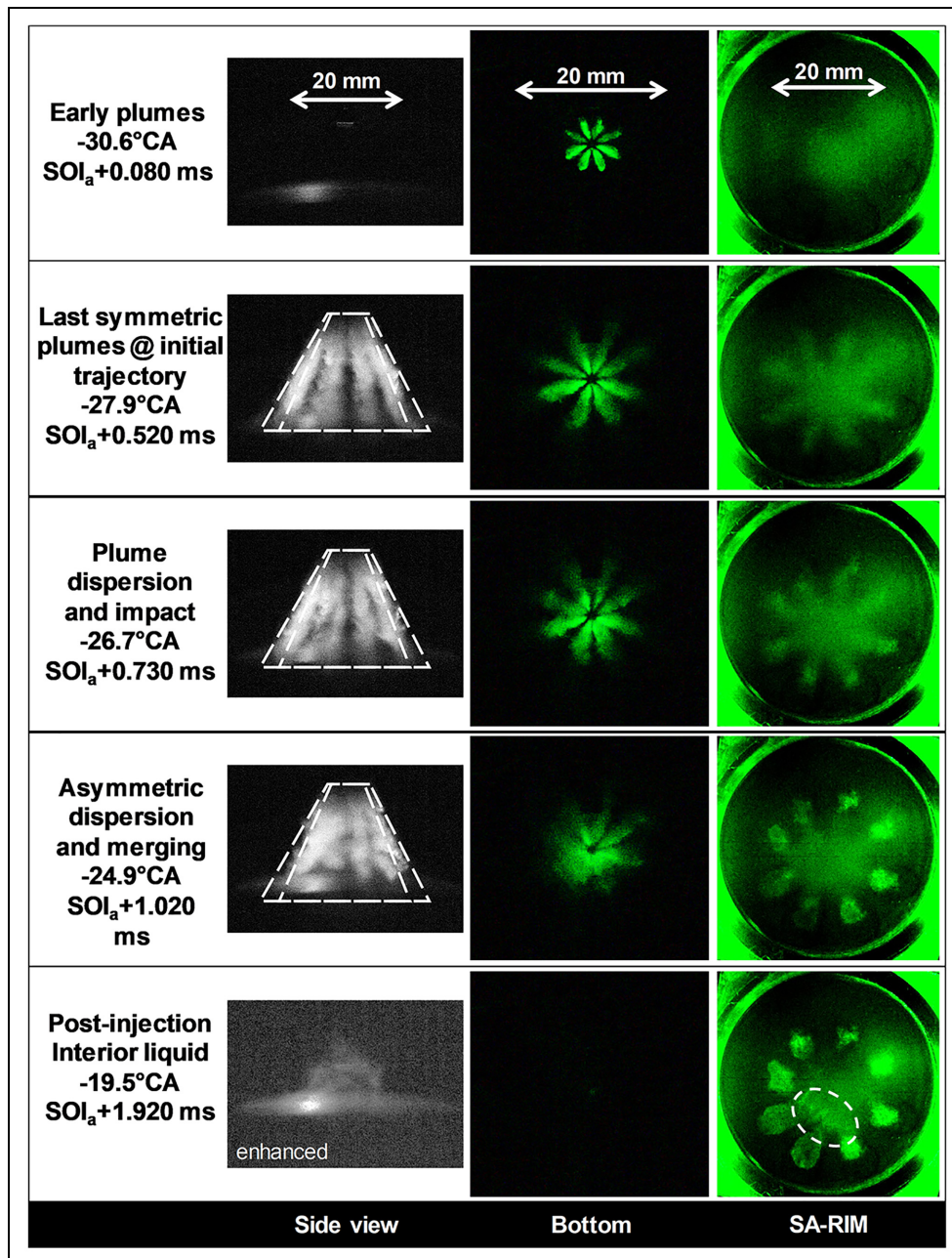
Figure 9. Images extracted from a single-cycle movie to illustrate the appearance of different stages during the spray evolution. Also, the SA-RIM images from separate tests at the same operating condition showing the fuel impact. Images are unprocessed except for enhancement (brightness and contrast) as noted in the one image. $SOI_a = -31$ °CA, injection duration = 1600 μs, $P_{in} = 100$ kPa.

ends of the obfuscated plume images. The plume-fuel impact is more clearly visible in the two later images. The higher image intensity of the fuel film (compared to the dry surface) demonstrates the second problem quantifying the volume from the SA-RIM compared to the LA-RIM; the imaged intensity can increase with fuel deposition rather than decreases as expected from surface scattered light alone (cf. section "SA-RIM") making volume quantification uncertain.

Nonetheless, the time and location of fuel deposition is unambiguous and can be related to the spray. It is clear that the fuel deposition from the plumes occurs

after −27.9 °CA and changes (presumably increasing the film volume) as this long injection continues. However, the films produced by the two merging jets at the 7 and 8 o'clock positions have less intensity and create a larger area than the others, which is consistent with having more dispersion of the liquid droplets. Long after the injection has ceased, −19.5 °CA, a fuel film has formed on the piston beneath the interior liquid below the two merged plumes (cf. dotted oval region). As with the spray-plume dispersion and merging, there is a notable asymmetry to the fuel-film formation. Furthermore, the deposition of the fuel from
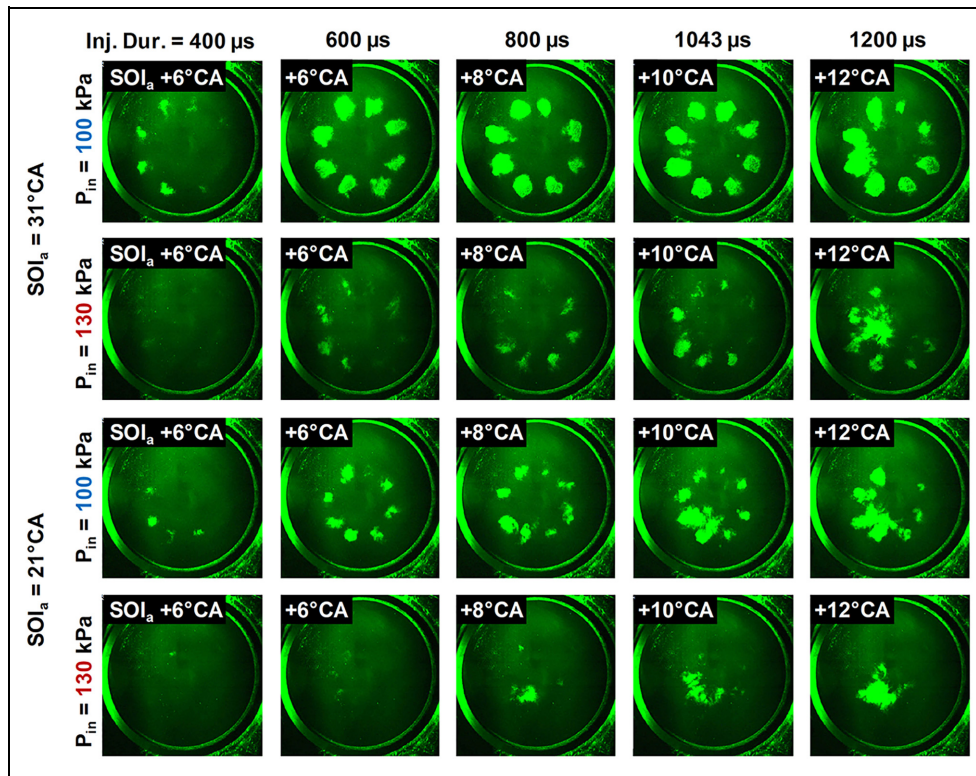
Figure 10. Fuel-film distributions after injection for different SOI$_a$, intake pressures, and injection durations.

the spray plumes and the deposition of the interior liquid can be separated in time.

Fuel-film variation versus engine operation

Density and temperature have been shown to markedly affect the spray development in quiescent chambers. Thus, it is of interest to systematically vary both in the engine to assess their effect on the fuel films. This is accomplished here by changing intake pressure, P_{in}, and injection timing; of course, the absolute values and rates of change cannot be changed independently. In addition, the injection duration is changed as this changes the length of the spray plumes, the amount of air required in the bowl to evaporate the fuel, and the time available for establishing the intra-plume flows which contribute to merging and collapse.

Figure 10 provides an overview of the fuel-film distributions recorded well after the injection event for SOI$_a$ = −31 °CA and −21 °CA, which span a range of reasonable values for this engine and single-injection strategy. The 100 and 130 kPa intake pressures are relevant for naturally aspirated and boosted operation, and injection durations from 400 to 1200 μs are relevant for part-load operation. The presented SA-RIM results were selected from individual single cycles. Figure 10 shows that increasing the injection duration at a given density (row) always increases the film areas for both the plume and interior fuel impacts, as is intuitive. At any given injection duration, increasing the

density by either P_{in} or SOI (top to bottom) decreases the area of the fuel deposited directly by the fuel plumes (cf. values in Figure 3). This is consistent with faster dispersion and evaporation of the plumes at higher density. For a fixed injection duration of 800 μs and higher, increasing density leads to the potential for the increased occurrence of fuel films formed by the interior fuel, albeit asymmetric as observed in the case of Figure 9. Interestingly, even though there is more air available in the bowl (due to higher density) for the same amount fuel, more of the interior fuel reaches the bowl window. Perhaps, because more of the fuel in the plumes is entrained to the interior at higher densities. This is examined further in Figure 11, where also images at two extreme values, SOI$_a$ = −41 °CA and −11 °CA, are shown. It is clear that the higher density (later injection) decreases the fuel impact by the plumes and increases the interior fuel impacting the window. Extrapolation from the spray sequence in Figure 9 suggests that the higher density is required to increase the rate of plume-fuel dispersion and subsequent entrainment to the interior.

Fuel area and volume versus engine operation

Another question that arises is the effect of the spray collapse on the amount of fuel deposited on the piston surface. For this reason, LA-RIM measurements were conducted to provide semi-quantitative information on the fuel-film thickness and volume. Operating
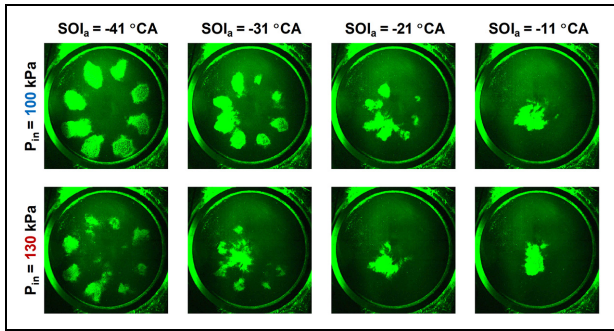
Figure 11. Fuel-film distribution after the injection event for 1200 μs injection duration, increasing gas density with retarded SOI_a.

conditions were chosen to match conditions used for fired engine tests (not reported here). For $P_{in} = 130$ kPa, the injection duration was 1395 μs and for $P_{in} = 100$ kPa, the injection duration was 1043 μs to maintain the same fuel-to-charge ratio for each P_{in}, corresponding to a supplied equivalence ratio (φ) of 0.33 for operation without exhaust gas recirculation (EGR). A sweep of injection timings was tested at each operating condition. The recorded intensity distributions were processed according to the steps described in section "LA-RIM."

The images in Figure 12 show the phase-averaged film height and standard deviation distributions of the

fuel films at the crank angle of maximum volume for an early and a late injection timing. The plots show the temporal evolution of the corresponding total phase-averaged areas. For either injection timing, the LA-RIM results demonstrate that the average fuel-film thickness is generally smaller for the higher intake pressure in spite of the longer injection duration (1395 μs vs 1043 μs).

At $SOI_a = -41$ °CA, the film patterns indicate that all spray plumes are distinct for $P_{in} = 100$ kPa whereas the beginning stages of plume merging and possibly collapse are indicated in the 7–8 o'clock positions for 130 kPa case. The standard deviation distributions show that a relatively low cycle-to-cycle variability of the fuel-film thickness is confined to the edges of the wetted area for the $P_{in} = 100$ kPa case. In contrast, $P_{in} = 130$ kPa results show cycle-to-cycle variability throughout the wetted area including the interior region. The increased standard deviation with pressure is consistent with the increased dispersion and entrainment observed in the sprays at higher densities. The increased cycle-to-cycle variability of the interior films is consistent with the spray entrainment being affected by the in-cylinder flow, which was demonstrated by the in-cylinder spray imaging of Zeng et al.[8] The area plots for early injection show that the fuel-film area is about the same for either intake pressure. For late injection with $P_{in} = 130$ kPa, a very low standard deviation of
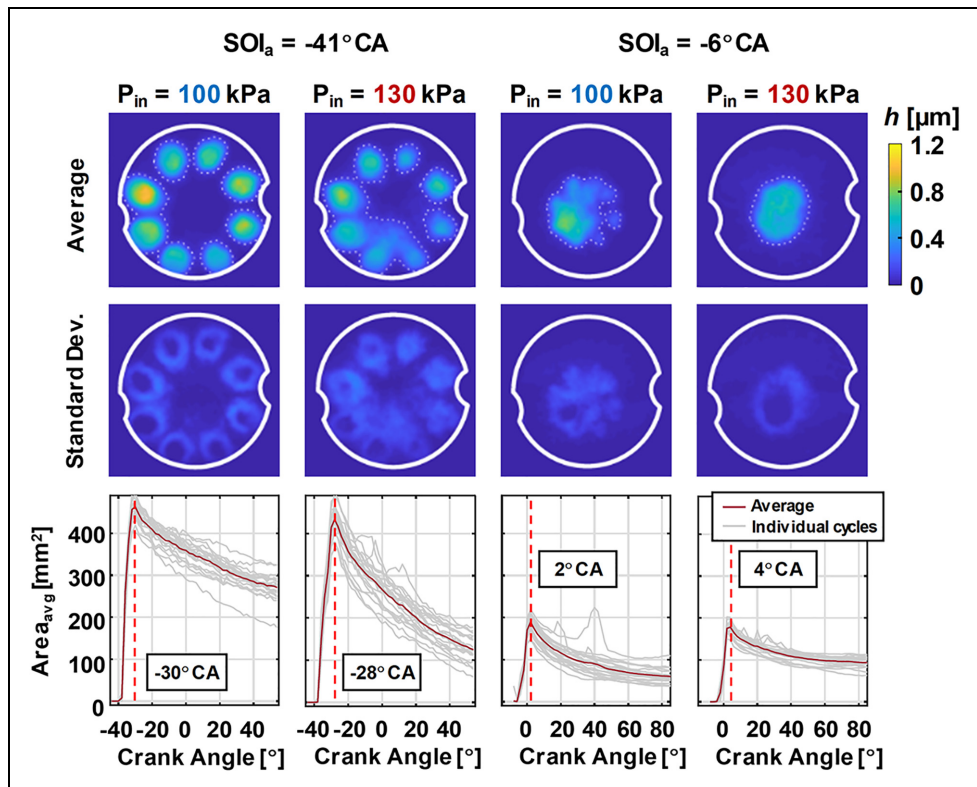

Figure 12. Top: Phase-averaged fuel-film thickness distributions at crank angle degree of maximum fuel-film area for two intake pressure and two SOI_a. Middle: Standard deviation maps. Bottom: Average fuel-film area evolution. Red dashed lines mark the crank angles selected for the fuel-film maps. $P_{in} = 130$ kPa used an injection duration of 1395 μs, and $P_{in} = 100$ kPa used an injection duration of 1043 μs, maintaining a supplied φ = 0.33.
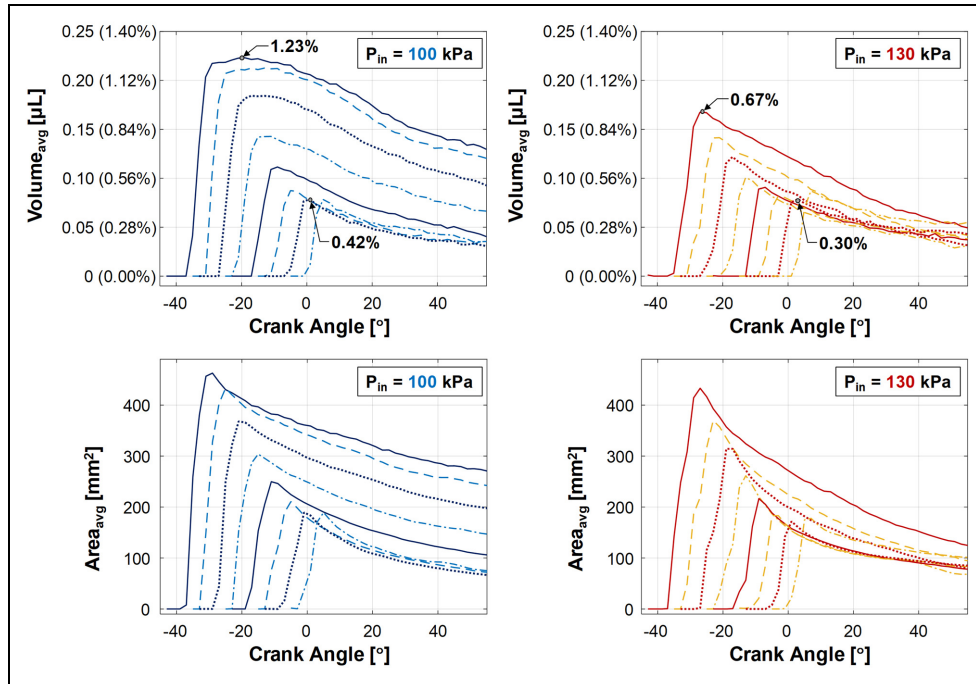
Figure 13. Fuel-film volume and area evolution for SOI$_a$ ranging from −41 °CA to −6 °CA in steps of 5 °CA. P$_{in}$ = 100 kPa used an injection duration of 1043 μs and P$_{in}$ = 130 kPa used an injection duration of 1395 μs.

the fuel film stands in contrast with the early injection. The difference could possibly be explained by a highly consistent spray collapse for the combination of high in-cylinder density (due to late SOI) and long injection duration.

The late injection timing (−6 °CA) indicates the direct impact of the plume-fuel between 1 and 5 o'clock only for the 100 kPa case, in spite of the close proximity of the piston. Furthermore, the film height is large and concentrated in the interior region. These two observations imply that increasing density by either intake pressure or late injection causes a more rapid plume dispersion and liquid entrainment to the interior of the spray.

Figure 13 shows the temporal evolution of the average fuel-film area for all investigated SOI$_a$ between −41 °CA and −6 °CA. The total film volume is also plotted, in both absolute and relative (percent of injected fuel) terms. A comparison of the peak values of the volume histories reveals that for early injection, the P$_{in}$ = 100 kPa case has much more fuel volume in fuel films, despite the shorter injection. By coupling this observation to the average fuel-film maps in Figure 12, it becomes clear that fuel impingement of the direct spray plumes is a relatively effective way to deposit fuel onto the piston top. It is of interest to relate the injected fuel volume to the amount of fuel detected on the piston-bowl window. To aid the interpretation of Figure 12, small circles and associated percentage numbers have been added to the peaks of the curves for the SOIs with largest and smallest volume. The largest fraction of deposited fuel is found for the SOI$_a$ = −41 °CA

case at P$_{in}$ = 100 kPa, for which approximately 1.2% of the injected fuel is detected as wall film. However, for the SOI$_a$ = −11 °CA case at P$_{in}$ = 130 kPa, only 0.3% of the injected fuel is deposited onto the piston-bowl window.

Furthermore, Figure 13 shows that for either intake pressure case, the maximum fuel-film area and volume decrease for retarded SOI$_a$ in the range of −41 °CA to −16 °CA. However, further SOI$_a$ retard in the range of −16 °CA to −6 °CA does not significantly change the fuel-film area and volume histories, except for a direct influence on the CA for which fuel deposition starts. A number of factors may be influencing this change in trend. As the piston approaches TDC, the piston speed is reduced; this causes the rate at which pressure and density increase as a function of time to drop. Consequently, the in-cylinder conditions are not significantly changed for the most retarded SOI$_a$ timings tested here (−6 °CA) compared to the next most retarded injection timing (−11 °CA).

In addition to the varying maximum fuel-film area and volume observed under varying injection timings, Figure 13 shows that the decay rates of the fuel-film area and volume are also highly variable between cases. While the area and volume decay rates are high for early injection timings at the P$_{in}$ = 130 kPa condition, the decay rates decrease significantly for retarded SOIs at this condition. At the most retarded SOI$_a$ (−6 °CA), the fuel-film area and volume decrease much more slowly, such that the resulting fuel-film areas and volumes at 55 °CA after TDC are very similar for all injection timings. In contrast, for P$_{in}$ = 100 kPa, the
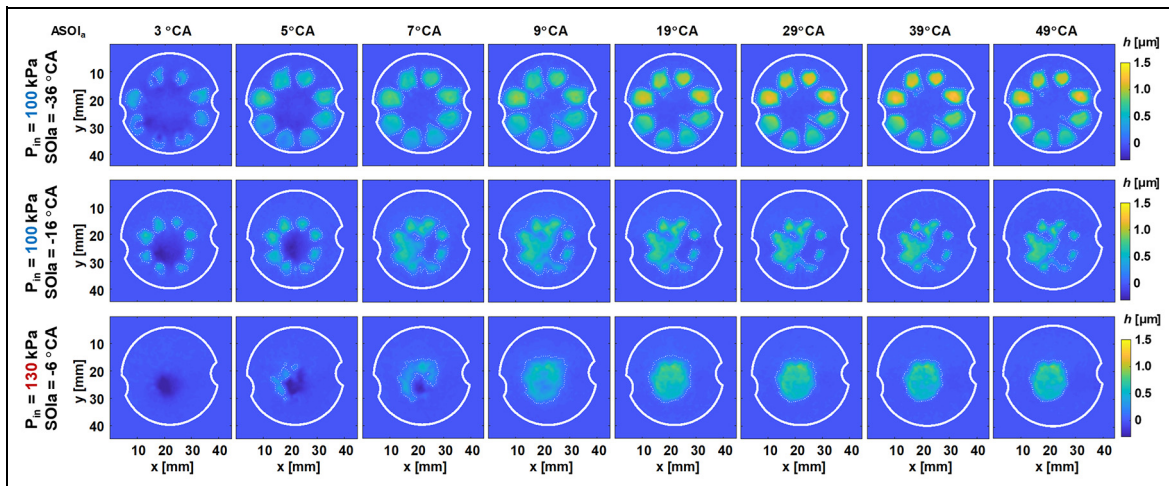
Figure 14. Temporal evolution of fuel film height for representative individual cycles.
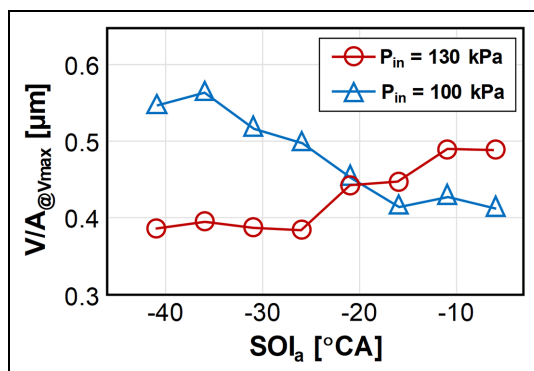

Figure 15. Average fuel-film height at the crank angle degree of maximum fuel-film volume for different injection timings SOI_a and intake pressures.

injection timing has a strong influence on both the fuel-film area and volume that remain at 55 °CA. For this condition, the decay rates remain unchanged with injection timing retard, which leads to substantial differences in the fuel-film area late in the cycle, as shown in Figure 13.

The previously described spray collapse plays an important role in this behavior. For the $P_{in} = 130$ kPa case, spray collapse starts to occur at earlier injection timings compared to the $P_{in} = 100$ kPa case due to the combination of longer injection and higher in-cylinder gas densities. At early injection timings, this causes the fuel film to be spread over a larger area due to the centered impingement at the end of the injection, as exemplified in Figure 12.

Figure 14 presents the temporal evolution of the fuel film at three different operating conditions which are representative of three distinct spray regimes: minimal plume interaction (top row), a transition regime leading to plume interaction and spray collapse (middle row), and a fully collapsing spray (bottom row). The minimal plume interaction example in Figure 14 results in eight distinct films on the piston surface. As the spray

targeting does not significantly change throughout the injection event, the temporal evolution primarily shows that these films grow in both height and radius as the plumes impinge on the piston, but the plumes do not merge, and this results in some areas with higher film thicknesses, and some outer areas of the films with low film thickness. The middle row of Figure 14 shows how the early part of the spray, prior to significant plume interactions, can result in distinct fuel films on the piston window. However, as the interaction between the plumes increases throughout the injection event, causing a minor spray collapse, this shifts the targeting of the fuel impingement and "sweeps" the surface of the piston window, resulting in a thin film over a large area. For later injection timings, the spray collapse is strong and the fuel impingement is concentrated in a central region, as shown in the bottom row of Figure 14. These variations in the fuel-deposit process result in different average fuel-film thicknesses, which are shown in Figure 15, as well as the varying decay rates of the fuel-film area and volume, which have already been discussed.

The average fuel-film thicknesses presented in Figure 15 have been calculated by dividing the fuel-film volume with the corresponding fuel-film area. The average fuel-film thickness displays opposite trends as a function of injection timing for the two intake pressures. For the $P_{in} = 130$ kPa case, the average fuel-film thickness is about 0.4 μm for early SOIs. For SOI_a later than −26 °CA, the average fuel-film thickness starts to increase. This corresponds well to the injection timings for which a strong spray collapse can be observed. For the $P_{in} = 100$ kPa case, the trend is different. For early SOIs, the average fuel-film thickness decreases from about 0.55 μm to slightly above 0.4 μm at $SOI_a = −16$ °CA. From there on, the average thickness remains constant for retarded injection timings. For the $P_{in} = 100$ kPa case, a strong spray collapse starts to occur at −16 °CA, which explains the changed trend at
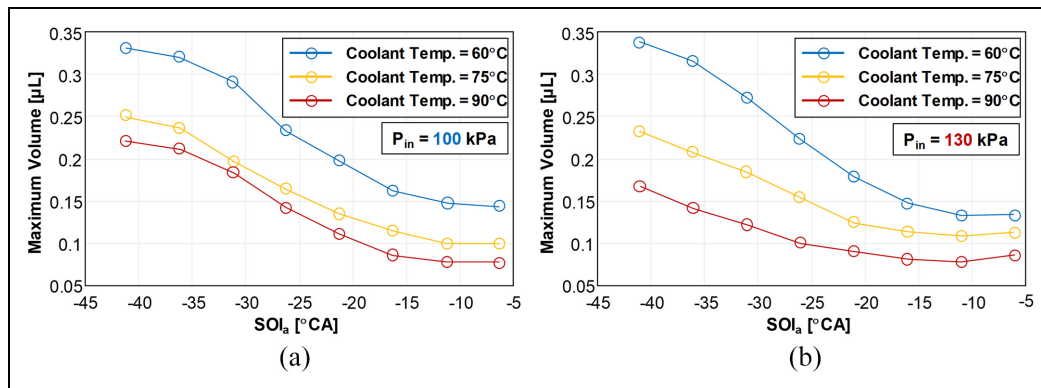
Figure 16. Maximum fuel-film volume generated by a range of injection timings at three coolant temperature levels and two intake pressures: (a) 100 kPa and (b) 130 kPa.

this injection timing. The average fuel-film thickness results highlight two important trends related to injection conditions. First, under lower initial-density conditions, which do not result in significant spray-plume merging and collapse, an incremental shift to a later SOI results in films with lower film areas and heights, despite a shorter distance between the injector and the piston. Here, the increased density and temperature outweigh the shorter distance. Second, under higher initial-density conditions, which result in significant spray collapse, retarded injection timings lead to reduced film areas, but thicker films, which can be more persistent throughout the cycle.

Effect of coolant temperature

Thus far, the interactions between spray dynamics and impingement on the formation of fuel films have been investigated under a range of in-cylinder conditions, which have been altered by start-of-injection phasing and intake pressure. These parameters are commonly used to control combustion phasing and engine mass flow rates, allowing optimization of efficiency and emissions as a function of the desired load. An additional parameter which may have a significant effect on engine performance is the coolant temperature. Although this parameter is controlled during normal operation, a significant transient period exists following cold-starts and following load transients when the coolant temperature is not at the desired steady-state value. Coolant temperature may be expected to have an impact on spray impingement because it will affect the in-cylinder temperature during the compression stroke by altering the mixture temperature prior to compression and during the compression stroke by changing wall-heat transfer dynamics. Therefore, a series of experiments were conducted with reduced coolant temperatures in order to study the effects of coolant temperature on spray impingement and wall fuel-film formation.

Figure 16 presents the maximum cumulative volume of the observed fuel films on the piston surface for each indicated SOI_a. Injection-timing sweeps were conducted

at three different coolant temperatures and two intake pressures. Figure 16 shows uniform results, in that lower coolant temperatures, under the interrogated conditions, always lead to a larger volume of fuel films. Also, the changes in coolant temperature do not significantly alter the trends observed under injection timing sweeps. This is particularly evident at the lower intake pressure condition, where a nearly constant offset in fuel-film volume is observed between each coolant temperature regardless of injection timing. This gives an initial indication that the spray dynamics are not significantly impacted by changes to coolant temperature, as the spray dynamics were found to underlie many of the fuel-film trends. However, further studies are required to confirm this hypothesis.

Figure 17 presents the average maximum-volume fuel-film height distribution for the six injection phasing sweeps which are presented in Figure 16. Figure 17 demonstrates the similar impingement spatial distributions which are generated for each injection timing and intake pressure. This suggests that the primary effect of the change in coolant temperature is a change in the volume of liquid reaching, and adhering to the piston top, rather than the spray dynamics, which would affect the spatial distribution of the fuel film, as shown previously in Figure 14. The fuel-film distributions in Figure 17 do demonstrate some slight differences in spatial distribution under certain conditions, such as with the $SOI_a = -16$ °CA, $P_{in} = 130$ kPa combination, where the 90 °C condition may indicate a greater degree of collapse than the 60 °C condition. However, many other cases exhibit nearly identical spatial distributions, with the primary differences in volume being derived from differences in the fuel-film height, such as is the case for the $P_{in} = 130$ kPa, $SOI_a = -31$ °CA condition.

Conclusion

It is generally accepted that fuel films on combustion chamber surfaces contribute significantly to engine-out PM emissions. Such films can be caused by direct-injection fuel-spray impingement on surfaces, and,
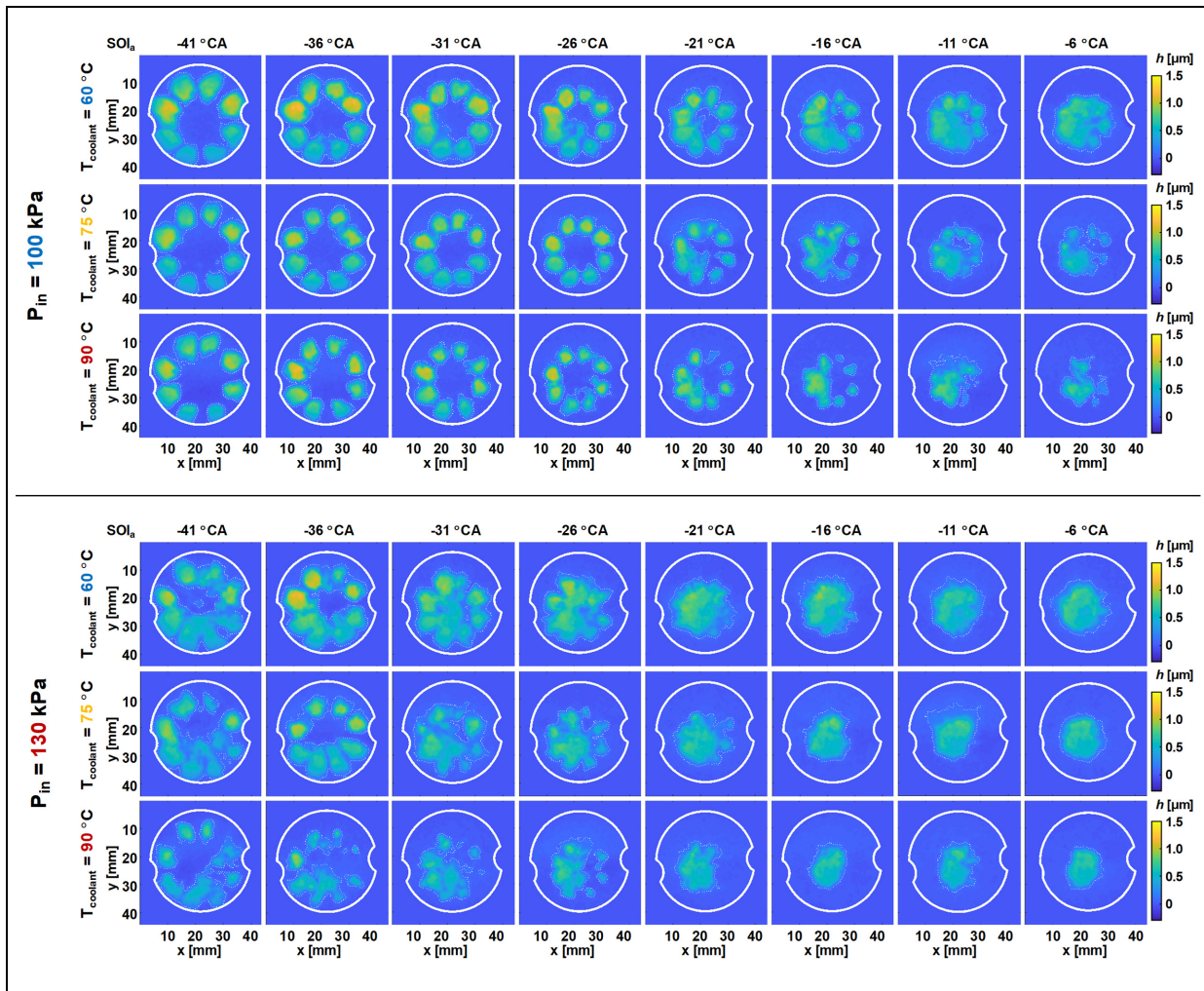
Figure 17. Phase-averaged fuel-film thickness distributions at the phasing of maximum average fuel volume for SOI_a sweeps at six combinations of coolant temperature and intake pressure.

depending on spray targeting, could occur on the piston top, cylinder head, or cylinder liner. This article systematically investigates the formation of fuel films on the piston of a light-duty spark-ignited engine operated in a motored fashion, mimicking a late injection stratified-charge combustion mode using a mid-level ethanol/gasoline blend (E30). The formation of fuel films was probed experimentally by probing both the direct-injection spray behavior and the resulting fuel films. The surface areas and thicknesses of fuel films were measured under a range of operating conditions using an optical diagnostic termed RIM. Fuel films occured at all of the operating conditions tested, which are common for DISI operation. However, the areas and volumes of the films exhibited strong dependencies within the tested operating conditions. The behavior was found to be non-monotonic, due to the contributions of competing trends. In particular, the peak film volume and area decrease with injection-timing retard (cf. Figures 13 and 16), whereas the average film thickness (Figure 15) increases at the boosted condition but

not the naturally aspirated. Apparently, there is a complex competition between the proximity of the piston to the injector and the higher gas temperatures and densities associated with injection timings close to TDC. In addition to these factors, the spray behavior markedly changed as a function of condition, with higher ambient temperature and density conditions leading to merging of the individual spray plumes and eventual "collapse" of the spray, which led to altered spray dynamics, including targeting and penetration. Therefore, depending on the particular regime of operation, altering injection timing or ambient density could either reduce or increase fuel-film area and volume.

There is a strong dependency of the fuel-film distribution, in terms of area and volume, on the evaporation of the fuel film after its formation. Unsurprisingly, fuel films with a higher area-to-volume ratio evaporated more quickly; importantly, the combined spray imaging and film linked the deposited film area-to-volume ratio to the spray behavior, with the state of

spray collapse being of chief importance. The study also involved variations of the engine coolant temperature. It was found that the primary effect of a reduced coolant temperature is the formation of thicker fuel films, with only minor changes to the fuel-film patterns. This suggests that the spray dynamics, in particular the degree of spray collapse, is not affected greatly by a change of the coolant temperature.

Overall, this article highlights the challenges when injecting fuel into the combustion chamber toward the end of the compression stroke and provides insight into the physical processes which govern fuel-film formation.

Future work

This article has investigated the spray dynamics and resulting piston-top fuel films of an E30 fuel in a stratified-charge DISI engine under a range of operating conditions. It has been shown that deviations from desired spray behavior, typified by increasing plume-to-plume interactions leading to spray collapse, can have a significant impact on spray impingement and fuel-film formation. Several areas of further research naturally arise from this work. First, it is clear that gasoline-spray plume-to-plume interactions and merging have significant effects on mixture formation, including fuel films. Although some of the physics relating to these phenomena are understood, a more holistic understanding is required to better anticipate and utilize the effects of plume-to-plume interactions. Also, for a majority of DISI engines, the fuel is injected during the intake stroke, motivating studies of spray formation and wall wetting for corresponding early injection conditions. Second, this article only probed a single fuel, and it is possible that fuels with varying physical properties, such as those with other bio-derived components, will have varying free-spray behaviors, and therefore varying plume-to-plume interactions. Therefore, similar investigations with a range of fuels should be conducted to better understand the sensitivity of the presented results to the particular E30 fuel that was used in this study. Finally, given the important role of CFD for engine-design efforts, future work should also assess the fidelity of spray and fuel-film submodels used in engineering CFD packages.

Declaration of conflicting interests

The author(s) declared no potential conflicts of interest with respect to the research, authorship, and/or publication of this article.

Funding

ORCID iD

Magnus Sjöberg https://orcid.org/0000-0002-4288-5607

References

1. Drake MC and Haworth DC. Advanced gasoline engine development using optical diagnostics and numerical modeling. *P Combust Inst* 2007; 31(1): 99–124.
2. Fansler TD, Reuss DL, Sick V and Dahms RN. Invited review: combustion instability in spray-guided stratified-charge engines: a review. *Int J Engine Res* 2015; 16(3): 260–305.
3. Zeng W, Sjöberg M, Reuss DL and Hu Z. High-speed PIV, spray, combustion luminosity, and infrared fuel-vapor imaging for probing tumble-flow-induced asymmetry of gasoline distribution in a spray-guided stratified-charge DISI engine. *P Combust Inst* 2017; 36(3): 3459–3466.
4. Drake MC, Fansler TD, Solomon AS and Szekely GA. Piston fuel films as a source of smoke and hydrocarbon emissions from a wall-controlled spark-ignited direct-injection engine. SAE technical paper 2003-01-0547, 2003.
5. Ding CP, Sjöberg M, Vuilleumier D, Reuss DL, He X and Böhm B. Fuel film thickness measurements using refractive index matching in a stratified-charge SI engine operated on E30 and alkylate fuels. *Exp Fluids* 2018; 59(3): 59.
6. Desoutter G, Cuenot B, Habchi C and Poinsot T. Interaction of a premixed flame with a liquid fuel film on a wall. *P Combust Inst* 2005; 30(1): 259–266.
7. Stevens E and Steeper R. Piston wetting in an optical DISI engine: fuel films, pool fires, and soot generation. SAE technical paper 2001-01-1203, 2001.
8. Zeng W, Sjöberg M and Reuss D. Using PIV measurements to determine the role of the in-cylinder flow field for stratified DISI engine combustion. *SAE Int J Engine* 2014; 7(2): 615–632.
9. Parrish SE, Zhang G and Zink RJ. Liquid and vapor envelopes of sprays from a multi-hole fuel injector operating under closely-spaced double-injection conditions. *SAE Int J Engine* 2012; 5(2): 400–414.
10. Blessinger M, Manin J, Skeen SA, Meijer M, Parrish S and Pickett LM. Quantitative mixing measurements and stochastic variability of a vaporizing gasoline direct-injection spray. *Int J Engine Res* 2015; 16(2): 238–252.

11. Sphicas P, Pickett LM, Skeen SA and Frank JH. Inter-plume aerodynamics for gasoline spray collapse. *Int J Engine Res* 2018; 19(10): 1048–1067.
12. Xu H, Wang C, Ma X, Sarangi AK, Weall A and Krueger-Venus J. Fuel injector deposits in direct-injection spark-ignition engines. *Prog Energ Combust* 2015; 50: 63–80.
13. Badawy T, Attar MA, Xu H and Ghafourian A. Assessment of gasoline direct injector fouling effects on fuel injection, engine performance and emissions. *Appl Energ* 2018; 220: 351–374.
14. Henkel S, Beyrau F, Hardalupas Y and Taylor AM. Novel method for the measurement of liquid film thickness during fuel spray impingement on surfaces. *Opt Express* 2016; 24(3): 2542–2561.
15. Alonso M, Kay PJ, Bowen PJ, Gilchrist R and Sapsford S. A laser induced fluorescence technique for quantifying transient liquid fuel films utilising total internal reflection. *Exp Fluids* 2010; 48(1): 133–142.
16. Schulz F, Samenfink W, Schmidt J and Beyrau F. Systematic LIF fuel wall film investigation. *Fuel* 2016; 172: 284–292.
17. Pan H, Xu M, Hung D, Lv H, Dong X, Kuo TW, et al. Experimental investigation of fuel film characteristics of ethanol impinging spray at ultra-low temperature. SAE technical paper 2017-01-0851, 2017.
18. Miyashita K, Tsukamoto T, Fukuda Y, Kondo K and Aizawa T. High-speed UV and visible laser shadowgraphy of GDI in-cylinder pool fire. SAE technical paper 2016-01-2165, 2016.
19. Geiler JN, Grzeszik R, Quaing S, Manz A and Kaiser SA. Development of laser-induced fluorescence to quantify in-cylinder fuel wall films. *Int J Engine Res* 2018; 19(1): 134–147.
20. Lin MT and Sick V. Mixture evaporative characteristics prediction for LIF measurements using PSRK (predictive Soave-Redlich-Kwong) equation of state. SAE technical paper 2002-01-2750, 2002.
21. Yang B and Ghandhi J. Measurement of diesel spray impingement and fuel film characteristics using refractive index matching method. SAE technical paper 2007-01-0485, 2007.
22. Maligne D and Bruneaux G. Time-resolved fuel film thickness measurement for direct injection SI engines using refractive index matching. SAE technical paper 2011-01-1215, 2011.
23. Zeng W, Sjöberg M and Reuss DL. Combined effects of flow/spray interactions and EGR on combustion variability for a stratified DISI engine. *P Combust Inst* 2015; 35(3): 2907–2914.
24. He X, Li Y, Sjöberg M, Vuilleumier D, Ding CP, Liu F and Li X. Impact of coolant temperature on piston wall-wetting and smoke generation in a stratified-charge DISI engine operated on E30 fuel. *P Combust Inst* 2019; 37: 4955–4963.
25. Fouts L, Fioroni GM, Christensen E, Ratcliff M, McCormick RL, Zigler BT, et al. *Properties of co-optima core research gasolines.* Technical report NREL/TP-5400-71341, August 2018. Golden, CO: National Renewable Energy Laboratory.